Cement and Concrete Research 40 (2010) 437–446

Contents lists available at ScienceDirect

Cement and Concrete Research

journal homepage: http://ees.elsevier.com/CEMCON/default.asp

Effects of calcination condition on expansion property of MgO-type expansive agent used in cement-based materials

Liwu Mo *, Min Deng, Mingshu Tang

College of Materials Science and Engineering, Nanjing University of Technology, Nanjing, 210009, China

ARTICLE INFO

Article history:
Received 30 December 2008
Accepted 25 September 2009

Keywords:
(A) Temperature
(A) Hydration
(B) Microstructure
(C) Expansion
(D) MgO

ABSTRACT

Previous research indicated that the expansion property of MgO-type expansive agent (MEA) depended strongly on the calcining conditions, i.e. kiln temperature and residence time. However, the intrinsic effect of calcination condition on the expansion property of MEA has not been clearly demonstrated. In the present work, the effects of calcination condition on the microstructure, hydration activity, and expansion property of MEA have been investigated, and their correlations are also studied. Results indicate that the microstructure of MEA is the intrinsic factor that controlling its expansion property, which is influenced by the calcination condition. MEA produced under higher temperature and longer residence time has less interior pores, larger crystal size of MgO, and smaller specific surface area, thus resulting in lower hydration activity and slower expansion at early age, but larger "ultimate" expansion at late age. While, a new expansion model of MEA is proposed to explain these results.

1. Introduction

Mitigating the shrinkage of cement-based materials is an important subject in modern cement materials science and technology. Much work has been focused on preventing the shrinkage of cement-based materials and many corresponding strategies have been developed [1]. Compensation for the shrinkage due to the expansion caused by the hydration of expansive additives, such as sulfoaluminate-type and CaO-type expansive additives, is one of the effective measures [2,3]. However, both of the aforementioned additives cause expansion mainly at early ages, usually being within 14 d, so some forms of shrinkage of cement-based materials such as drying shrinkage and thermal shrinkage generated at later ages would not be compensated effectively. For sulfoaluminate-type additives, large volume of water is needed for the formation of its hydration product, ettringite, which hinders its application in some structures without enough moisture curing or some high performance concretes with low w/c in which it is hard for the penetration of exterior water into the interior portion of concrete. Additionally, ettringite may undergo decomposition at high temperature (over 70 °C) [4,5], so it may be unsuitable for some massive concrete with a high temperature rise. Compared to those expansive additives, the hydration of MgO needs less water, and its hydration product, $Mg(OH)_2$, is more stable in cement paste. Thus it could be applied more widely in modern concrete as a shrinkage-compensating additive.

Expansion due to the slow hydration of intrinsic MgO in cement was first noticed as it cracked the cement matrix, and thus the content of MgO in cement was limited in many cement specifications [6]. However, the expansion caused by the hydration of MgO, if it is controlled, could also be used to compensate the shrinkage of cement-based materials. Mehta [7] reported that the carefully calcined (under the temperatures of 900–950 °C) and sized (300–1180 μm) MgO powders had the potential of being used as expansive agents for compensating thermal shrinkage and thus preventing cracks in mass concrete due to thermal stresses. But this kind of MgO was not produced industrially and applied in mass concrete. In the 1970s, the Baishan dam was constructed by using cement with high MgO (4.5% by mass of cement) in China, and no temperature-controlling measures were taken during the constructing process [8]. Several years later, no penetrating cracks were found. Subsequent studies indicated that the thermal shrinkage of dam concrete generated during the cooling stage has been effectively compensated by the delayed expansion attributed to the slow hydration of MgO in cement. From then on, much research has been focused on the application of delayed expansion due to the hydration of MgO in compensating thermal shrinkage of mass concrete, and many dams were constructed using this kind of cement with high MgO content to reduce or even cancel the temperature controlling measures [8]. As the clinkering temperature of cement is about 1400 °C, the MgO is always dead-burnt, resulting in very slow hydration rate [6]. To avoid dead burnt MgO in cement for good control of the properties of MgO, some Mg-bearing minerals such as magnesite and dolomite were calcined separately under much lower temperatures ranging from 900 °C to 1200 °C to produce MgO-type expansive agent (MEA) [8–10]. Some researches indicated that the expansion

* Corresponding author. Tel.: +86 25 83587218.
E-mail addresses: andymoliwu@sohu.com (L. Mo), dengmin@njut.edu.cn (M. Deng).

0008-8846/$ – see front matter © 2009 Elsevier Ltd. All rights reserved.
doi:10.1016/j.cemconres.2009.09.025

properties of MEA depended on the calcining temperature and residence time. For example, MEA produced under higher calcining temperature, resulted in slower and smaller expansion at early age but larger expansion at later age [9]. However, why the MEA calcined under different calcination condition have different expansion properties has not been clearly demonstrated. According to the previously proposed expansion mechanism of MgO in cement, such as the swelling pressure and crystal growth pressure [11–13], the fact that more delayed expansion is generated by MEA calcined under higher temperature could not be well explained.

The present work aims to find out the intrinsic effects of calcination condition on the expansion property of MEA through correlating the calcination condition to its microstructure, hydration activity and expansion properties. Thus the microstructure, activity and expansion properties of MEA produced under different calcination condition were investigated. Finally, the different expansion behaviors of MEA produced under different calcination condition are explained by a new expansion model of MEA proposed according to its hydration and expansion characteristics in cement paste.

2. Experimental

2.1. Preparation of MEA

Magnesite from Liaoning Province, China, has been used as raw materials. Its chemical composition is shown in Table 1 and the X-ray diffraction (XRD, 40 kV × 40 mA,Cu-Kα radiation) patterns are shown in Fig. 1. The magnesite was crushed and ground into fine particles with size less than 80 μm. It was then calcined in an electric furnace at a given temperature, and after a given residence time, the sample was cooled in air. After calcination, MEA were ground in a mortar and passed a sieve with mesh of 0.08 mm to make sure the particle size of MEA be in the range of 0–80 μm. The calcination temperatures varied from 900 °C to 1300 °C and residence time were 0.5 h, 1.0 h, or 1.5 h. The specific calcination regimes are shown in Table 2. As shown in Fig. 2, the MEA consists mainly of MgO. For S900-1.0 (i.e. the sample calcination temperature was 900 °C and the residence time was 1.5 h), there is an obvious characteristic peak of magnesite in the X-ray diffraction patterns (Fig. 2) and significant LOI (loss on ignition) (Table 2), implying some magnesite has not been decomposed. With the increase of temperature and residence time, the LOI decreases and the MgO content increases (Table 2), indicating the magnesite approaches complete decarbonation.

2.2. Microstructure characterization

The morphology of MEA was examined by Scanning Electron Microscope (SEM, JSM-5900, JEOL, Ltd., Japan). The average crystallite size of MgO was determined by X-ray diffraction using the line broadening of the six strongest peaks of MgO (JCPDS card # 4-0829). The profile was fitted with the Lorentzian (Cauchy) function. And thus the full width at half maximum (FWHM) was determined after correcting the instrumental broadening. Finally, the Scherrer equation [14] was used to calculate the average crystallite size. The specific surface area of MEA was tested by N_2 adsorption (BET measure). And the pore structures of MEA were characterized by using a Micromeritics ASAP 2020 volumetric instrument. The test range of pore radius was from 2 nm to 50 nm.

Table 1
Chemical compositions of the magnesite.

Raw material	Chemical compositions/wt.%								
	MgO	CaO	SiO_2	Al_2O_3	Fe_2O_3	Na_2O	K_2O	SO_3	LOSS
Magnesite	45.68	1.46	1.76	0.32	0.79	–	–	–	48.77
Cement	0.94	64.45	19.5	4.78	3.43	0.28	0.40	2.48	2.91

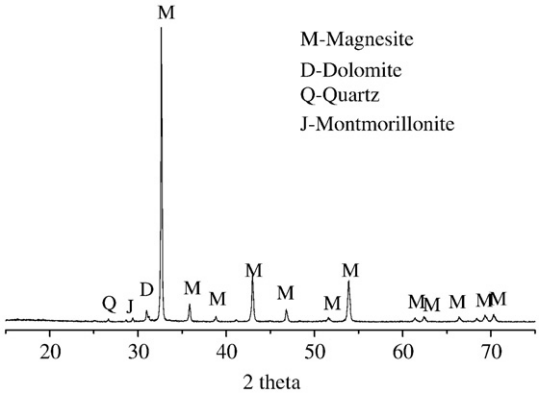

Fig. 1. X-ray diffraction patterns of the magnesite.

Density of MEA was determined referring to the test method of cement density described in the standard of GB/T 208-1994 [15], in which the MEA was immersed into coal oil and the density was calculated by Archimedes' principle.

2.3. Hydration activity determination

The neutralization time, which was determined by using 1.70 ± 0.1 g of MEA to completely neutralize 200 mL of 0.07 mol/L citric acid solution at 30 ± 1 °C, was taken as a measure of evaluating the activity of MEA. Obviously, shorter neutralization time means higher activity.

MEA were mixed respectively with water at the water/MEA ratio of 10:1 in breakers and cured at 20 ± 2 °C. The mixture was sampled at different intervals and washed by absolute alcohol to stop the hydration. Then the micro-morphologies of hydration products were examined by SEM. The hydration degree of samples was calculated by Eq. (1) according to the mass loss of sample due to dehydration of $Mg(OH)_2$ determined by Thermogravimetric analysis and Differential Scanning Calorimetry analysis (TG-DSC).

$$d = \frac{L_{Mg(OH)_2} * (40/18)}{C} \quad (1)$$

where, d, $L_{Mg(OH)_2}$ and C represent the hydration degree, mass loss ratio due to the dehydration of $Mg(OH)_2$ and the content of MgO in MEA respectively.

Table 2
Chemical compositions of MEA calcined under different conditions.

Sample	Calcination condition		Chemical compositions / wt.%					
	Temperature /°C	Time /h	MgO	SiO_2	Fe_2O_3	Al_2O_3	CaO	Loss
S900-0.5	900	0.5	78.56	3.68	0.64	0.59	2.33	14.20
S900-1.0	900	1.0	80.95	4.35	0.97	0.58	2.41	8.83
S900-1.5	900	1.5	87.65	4.90	1.01	0.57	2.21	2.03
S1000-0.5	1000	0.5	88.05	4.45	1.86	0.55	1.96	3.83
S1000-1.0	1000	1.0	89.29	4.86	1.02	0.58	2.13	2.11
S1000-1.5	1000	1.5	90.35	4.88	1.00	0.56	2.23	1.03
S1100-0.5	1100	0.5	89.79	4.67	1.06	0.54	2.31	1.63
S1100-1.0	1100	1.0	89.24	4.30	0.98	0.55	2.34	0.64
S1100-1.5	1100	1.5	90.36	4.26	0.99	0.54	2.30	0.56
S1200-0.5	1200	0.5	90.23	4.22	1.04	0.57	2.28	0.31
S1200-1.0	1200	1.0	91.08	4.21	0.92	0.56	2.08	0.02
S1200-1.5	1200	1.5	91.63	4.31	1.03	0.46	2.16	0.04
S1300-0.5	1300	0.5	91.56	4.28	1.06	0.49	2.22	0.05
S1300-1.0	1300	1.0	91.94	4.03	0.90	0.55	2.35	0.03
S1300-1.5	1300	1.5	92.01	4.14	0.89	0.56	2.34	0.03

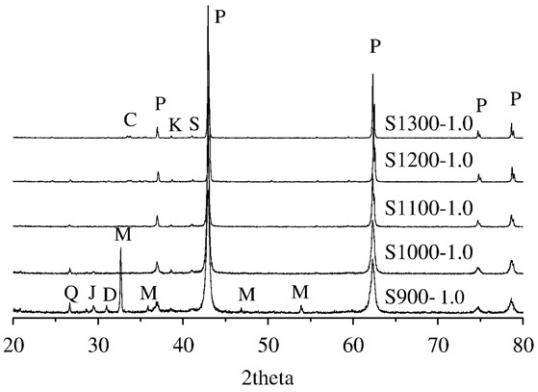

Fig. 2. X-ray diffraction patterns of MEA (calcined respectively at 900 °C,1000 °C, 1100 °C, 1200 °C, and 1300 °C for 1.0 h; P — Periclase, M — Magnesite, D — Dolomite, Q — Quartz, J — Montmorillonite).

2.4. Expansion of cement paste containing MEA

Type P.II 42.5 Portland cement produced by Jiangsu-Onada cement Corp., Nanjing, China was used. Its chemical composition is shown in Table 1. Eight percent of MEA by the weight of cement was first mixed into cement, then mixed with water at the water/binder ratio of 0.30 to obtain a homogeneous mixture. The mixtures were cast into 20 mm 20 mm 80 mm moulds, and then cured in a standard curing room with RH≥95%, 20±1 °C for 24 h. After then, these specimens were demoulded and cured in water at 20 °C and 40 °C after measuring the initial lengths. The length changes of cement pastes were measured periodically.

2.5. SEM analysis on the hydration products of MEA in cement paste

In order to investigate the hydration characteristics of MEA in cement paste, fractured surface of the hydrated MEA particle contained in cement paste at age of 270 d cured in water at 40 °C was sampled and investigated by SEM. Thin prisms were sawn from the center portions of cement paste using a precision diamond saw and a non-aqueous lubricant. They were then dried, impregnated with epoxy resin, hardened, and finally polished in the usual manner [16] for backscatter SEM examination, and then the polished samples were investigated by backscatter SEM.

3. Results and discussion

3.1. Microstructures of MEA

Fig. 3 shows SEM micrographs of MEA prepared under different calcination conditions. These figures illustrate that a single particle of MEA consists of many aggregated MgO grains, and the size of MgO grain increases with the increasing temperature and residence time. The grain growth of MgO is attributed to the sinter of MgO at the high temperature. During calcining, the magnesite first decomposes into MgO microcrystal, and the microcrystal then sinters under the high temperature, causing grain growth of MgO. Kleiman et al. [17] found that MgO grains underwent coarsening already at temperature as low as 0.31 of the MgO melting point (3125 K), namely being about 700 °C.

With the growth of MgO grain, the arrangement of atoms in MgO become more regular, thus decreasing the crystal defects in MgO. As shown in Table 3, with the increase of temperature and residence time, the average crystal grain size of MgO increases, while the lattice

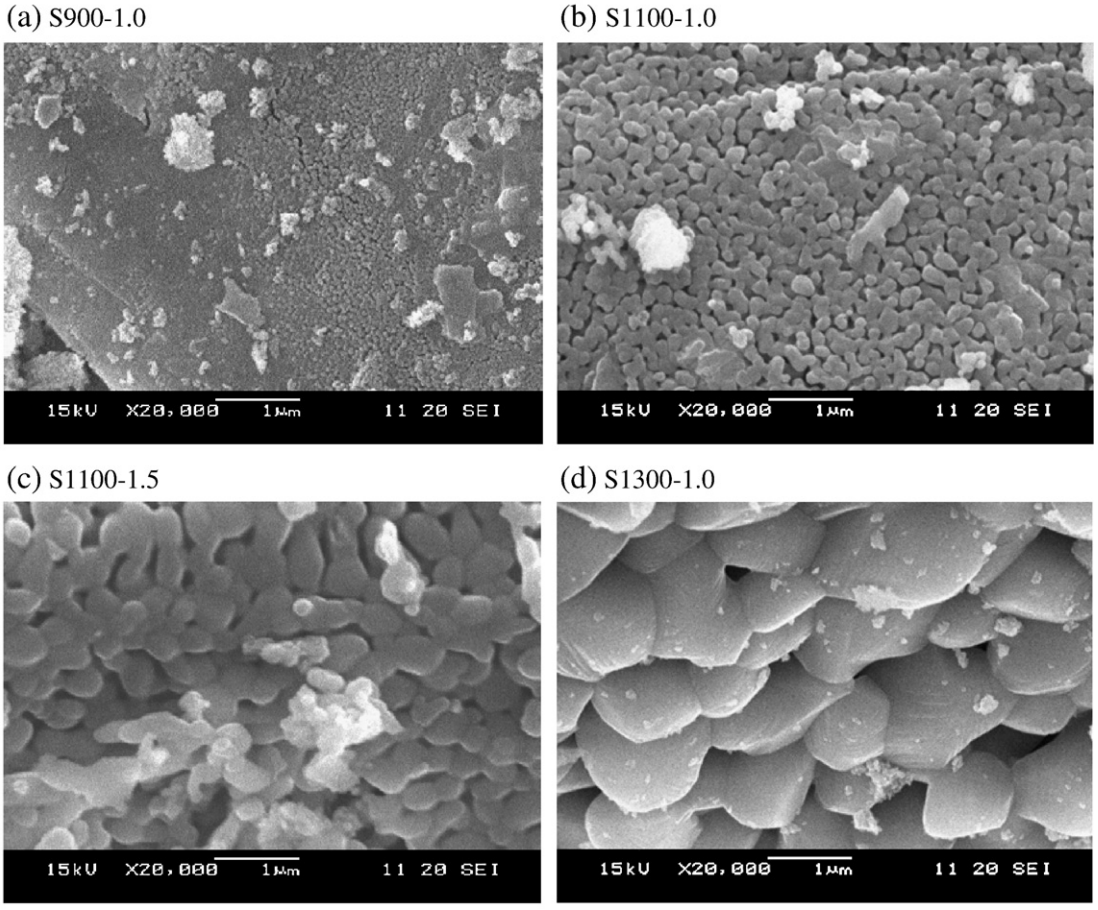

Fig. 3. Effect of calcination temperature and residence time on the morphology of MEA.

Table 3
Crystal grain size and lattice distortion of MgO, specific surface area, interior pore volume, pore width and density of MEA calcined under different calcination conditions.

Sample	Crystal grain size (nm)	Lattice distortion (%)	Specific surface area (m^2/g)	Pore volume (cm^3/g)	Average pore width (nm)	Density (g/cm^3)
S900-0.5	21.2	0.1648	52.7	0.193	14.62	2.97
S900-1.0	29.3	0.0560	55.2	0.223	16.10	3.02
S900-1.5	36.8	0.0350	45.9	0.179	15.57	3.12
S1000-0.5	30.4	0.0208	49.8	0.235	18.84	3.13
S1000-1.0	43.2	0.0149	39.8	0.235	23.61	3.26
S1000-1.5	66.3	0.0092	18.9	0.103	25.12	3.32
S1100-1.0	>100	–	4.2	0.024	22.46	3.43

distortion of MgO decreases. This agrees with the results reported by Sun et al. [18], who also found that the lattice distortion of MgO crystal decreased with the growth of MgO crystal grain. When the crystal grain size of MgO is larger than 100 nm, the Scherrer equation is not suitable to be used for the crystal size calculation.

Fig. 4 shows the effects of temperature and residence time on the internal specific surface area. Obviously, specific surface area of MEA decreases with the increase of temperature and residence time. This may be closely related to the grain growth of MgO. During the decomposing process of magnesite, porous structures are first formed as CO_2 escapes, and then the MgO grains grow due to the continued sintering of MgO, causing reduction of total pore volume and enlargement of pore size, and thus decreasing the specific surface area (Table 3). As shown in Table 3, S1000-0.5 and S1000-1.0 have the same total pore volumes, but the latter has smaller specific surface area due to its larger the pore size. Although the residence time for S900-1.0 is longer than that for S900-0.5, the former has larger specific surface area. This may be ascribed to the higher content of MgO in S900-1.0 (Table 2). As shown in Table 3, the density of MEA increases with the increase of calcination temperature and residence time.

3.2. Hydration activity of MEA

Fig. 5 shows the neutralization times of MEA calcined under different conditions. For the same residence time, the neutralization time increases with the increasing temperature, indicating the hydration activity of MEA decreases with the increasing temperature. Longer residence time also causes longer neutralization time of MEA. At higher temperature, the residence time has stronger influence on the neutralization time. For example, when the residence time is increased from 0.5 h to 1.5 h, 24 s of the neutralization time of MEA is increased at the calcination temperature of 900 °C, while 81 s and 400 s are increased at 1000 °C and 1100 °C respectively.

As reported in Section 3.1, the MgO used as expansive agent is polycrystalline and could generally be described as sinter bonded single MgO grains. Hydration activity of MEA depends both on the area of reaction region and the activity of MgO grain. The former is related closely to the specific surface area, and the latter depends strongly on the crystal structures of MgO. Fig. 6 shows the relationship

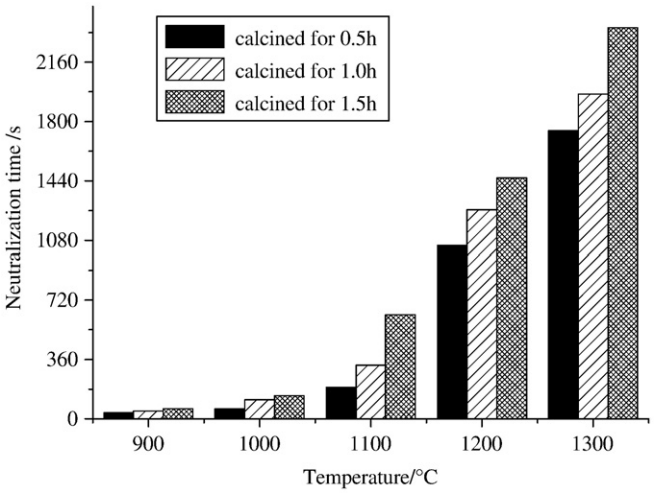

Fig. 5. Effect of calcination temperature and residence time on the neutralization time of MEA.

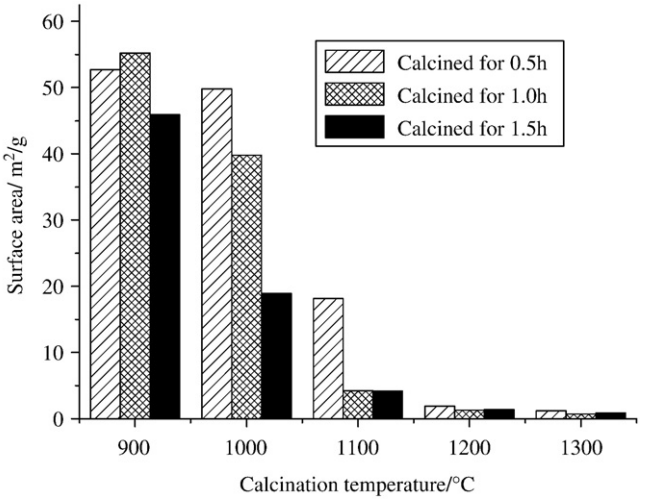

Fig. 4. Effect of calcination temperature and residence time on the specific surface area of MEA.

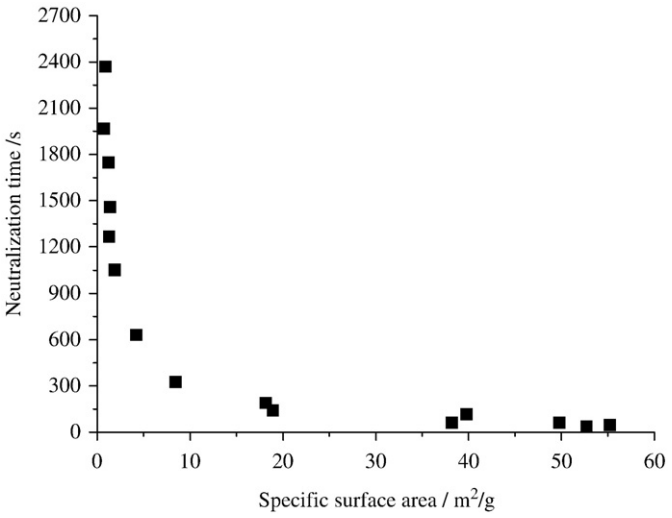

Fig. 6. Relationship between the specific surface area and the neutralization time of MEA.

between the specific surface area and the neutralization time of MEA. As show in Fig. 6, the neutralization time decreases with the increasing specific surface area. When the specific surface area is less than about 1.3 m^2/g, the neutralization time decreases largely with the increasing specific surface area, but it decreases less apparently when the specific surface area increases to larger than about 20 m^2/g. This may be ascribed to that, besides the surface area, the hydration activity of MgO grain which is related to its crystal size also has influence on the activity of MEA. Wogelius et al. [19] reported that the hydration activity of MgO was related to its surface structures, MgO with low-defect surface has lower activity. At early stage of sintering, many defects exist in MgO, and thus the activity of MgO grain is very high. With the grain growth of MgO, the array of atoms in the crystal lattice of MgO becomes gradually regular, and thus decreases the crystal defects, resulting in the decrease in hydration activity. In addition, the grain boundary (interface of MgO grain) of MgO has higher free energy, which is more likely to react with water [19]. However, this kind of interface also decreases with the grain growth of MgO.

Fig. 7 shows the SEM images of S900-1.0, S1100-1.0, and S1300-1.0 hydrated in water as illustrated in Section 2.3. Their neutralization times are 46 s, 325 s, and 1966 s, and they are renumbered as MEA-46, MEA-325, and MEA-1966 respectively. MEA-46 hydrates most rapidly, large number of hexagonal platelets of $Mg(OH)_2$ have already been formed at 2 d (Fig. 7(a)), and about 97.05% of MgO has been hydrated (Table 4). At 7 d, all of the MgO has been completely

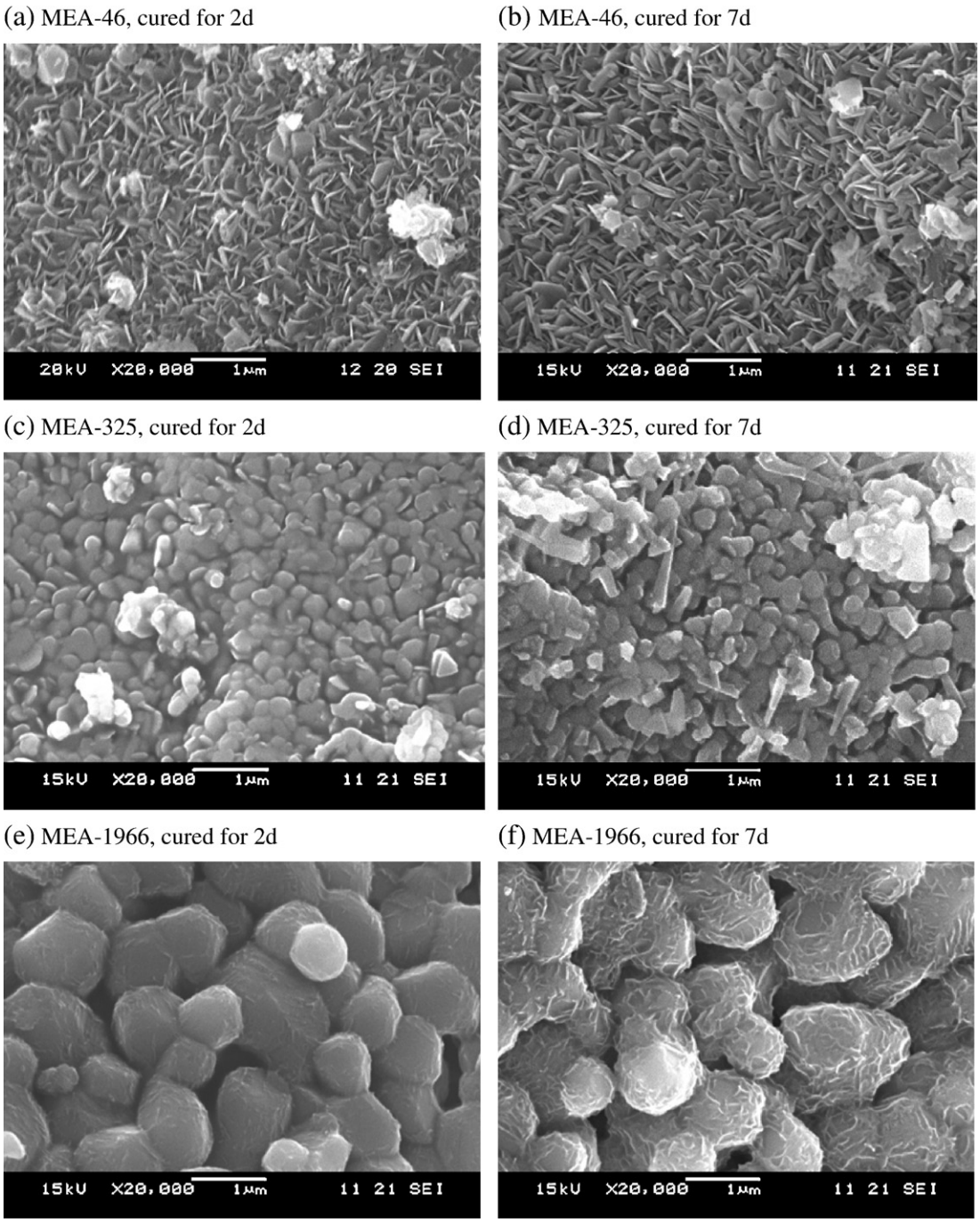

Fig. 7. SEM image of the hydration products of MEA-46, MEA-325, and MEA-1966 cured in water at 20 °C.

Table 4
Hydration degree of MgO in MEA cured in water at 20 °C.

Sample	Neutralization time (s)	Hydration degree of MgO (%)			
		2 d	7 d	15 d	30 d
S900-1.0	46	97.05	100	100	100
S1100-1.0	325	4.53	9.90	20.89	82.59
S1300-1.0	1966	–	0.98	1.93	7.86

hydrated, and the platelet thickness of $Mg(OH)_2$ increases (Fig. 7(b)). For MEA-325, a few fine sheet $Mg(OH)_2$ has been formed at the age of 2 d, and some products are filled in the pores (Fig. 7(c)), the corresponding hydration degree of MgO being 4.53%. At 7 d, the $Mg(OH)_2$ growth increases (Fig. 7(d)) and the hydration degree increases to 9.90%. MEA-1966 hydrates most slowly, at 2 d, only some lamellar $Mg(OH)_2$ is formed on the surface of MgO grain, especially on the boundary of MgO grains (Fig. 7(e)), indicating the surface and the boundary of MgO grains have begun to react with water. At 7 d, the hydration products increased, covering the surface of MgO grains (Fig. 7(f)), but still only 0.98% of MgO has been hydrated. According to the above results, the hydration activity of MgO grain seems to play a more important than the surface area in the hydration activity of MEA.

3.3. Expansion property of MEA

Five kinds of MEA with different neutralization times of 46 s (S900-1.0, re-numbered as MEA-46), 115 s (S1000-1.0, re-numbered as MEA-115), 325 s (S1100-1.0, re-numbered as MEA-325), 1266 s (S1200-1.0, re-numbered as MEA-1266), and 1966 s (S1300-1.0, re-numbered as MEA-1966) were added into cement paste. Fig. 8(a) shows the expansion curves of cement pastes containing MEA cured at 20 °C in water. Cement paste with MEA-46 expands most rapidly, but after 70 d, the expansion curve levels off. Cement paste with MEA-115 shows similar expansion, but its expansion is slightly less than that of MEA-46 before 70 d and slightly greater after 70 d. Cement paste with MEA-325 expands continuously–initially more slowly, but after 240 d, its expansion exceeds that caused by MEA-46 and MEA-115. The expansion caused by MEA-1266 and MEA-1966 is very slow compared to MEA-46, MEA-115 and MEA-325.

Fig. 8(b) shows the expansion curves of cement pastes containing MEA cured in water at 40 °C. Evidently, the expansion of cement paste is greatly accelerated. The expansion curves of cement pastes added with 8% of MEA-46, MEA-115, and MEA-325 level off at 14 d, 30 d, and 70 d respectively. In the case of MEA-46 and MEA-115, the corresponding "ultimate" expansions are about 0.22% and 0.28%, which is similar to the "ultimate" expansions at 20 °C. Before 14 d, the expansion caused by MEA-325 is smaller than that caused by MEA-46 and MEA-115 at equivalent age. But, after 14 d, the expansion caused by MEA-325 exceeds that caused by the later two. For MEA-1266, its expansion is very slow at early age, but a knee point occurs on the expansion curve at 70 d, and from then on, the expansion was drastically accelerated. MEA-1966 has the slowest expansion at early age. There is again a knee point on the expansion curve, occurring at the age of 120 d, and then the expansion is accelerated.

Results indicate that MEA with higher activity (shorter neutralization time) will produce rapider and larger expansion at early age, and the expansion curves level off at earlier age. While MEA with lower activity (longer neutralization time) will produce slower and less expansion at early age, but rapider and larger expansion at late age, and the time needed for the expansion curve to flatten is longer. In addition, when cured at 40 °C, the expansion of MEA with low activity is accelerated after an induction period. The lower the activity of MEA is, the longer the induction period will be.

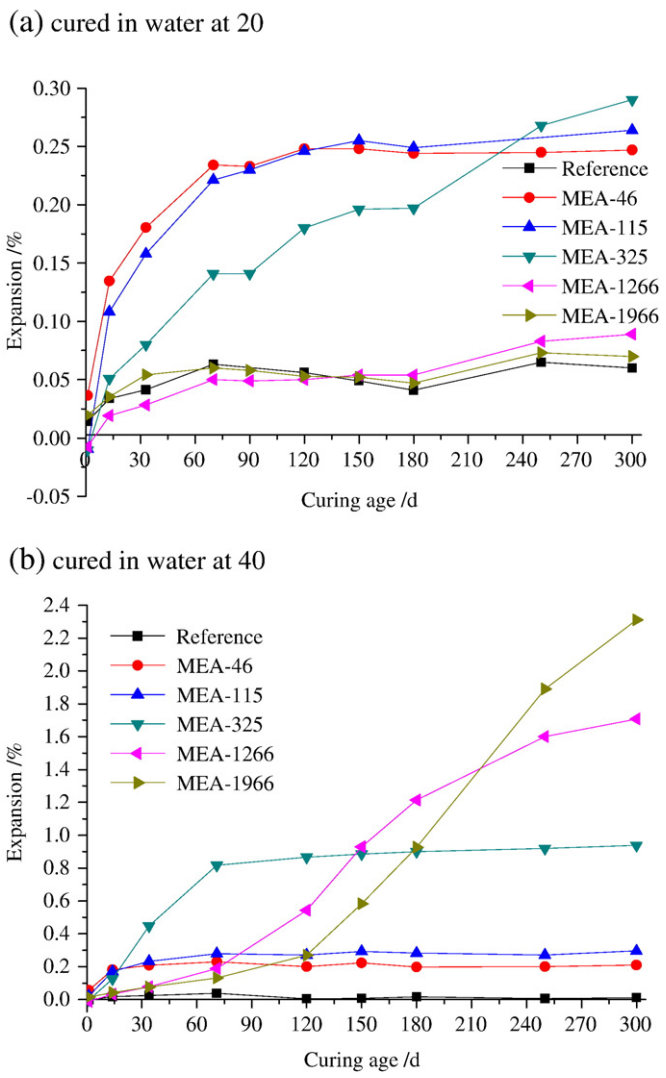

Fig. 8. Expansion curves of cement pastes containing 8 wt.% of MEA with different neutralization time.

3.4. Hydration products of MEA in cement paste

Figs. 9–11 show the SEM images of the fracture surface of MEA particles of MEA-46, MEA-325, and MEA-1966 embedded in cement pastes. As shown in these figures, the size of hydration products $Mg(OH)_2$ are much smaller than that hydrated in water and the SEM morphology of $Mg(OH)_2$ are irregular. This may be related to the effect of alkali on the hydration of MgO in cement paste. It was reported that the alkali affected the supersaturation, hydration rate, the sites of nucleation and growth, and the morphology of $Mg(OH)_2$ [13,20]. Due to the high concentration of OH^- in the pores of cement paste, the diffusion distance of Mg^{2+} produced during the hydration is shorten, and supersaturated solution of Mg^{2+} and OH^- ions is generated near the hydration site, and thus the $Mg(OH)_2$ is formed locally at the sites of MgO grain, or formed in a confined region near the sites of MgO grain after short-range diffusion of Mg^{2+} [13]. As seen in Fig. 11, cracks are induced at the interface of sintered MgO grains, this may be related to the expansion at the grain boundary of MgO, breaking apart the sintered MgO grains.

Fig. 12 shows the backscatter image of MEA-1966 particle embedded in cement paste cured in 40 °C at the age of 270 d. It illustrates that the MEA particle is surrounded by the cement

(a) MEA-46 particle embedded in cement paste

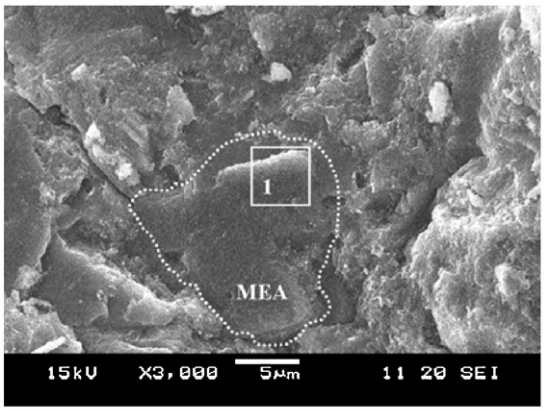

(b) Higher magnification image of zone 1

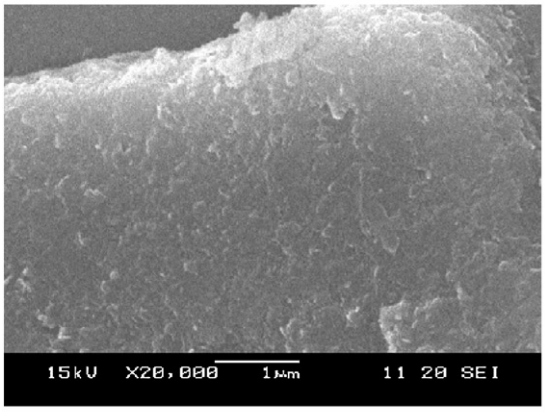

(c) EDS of zone 1

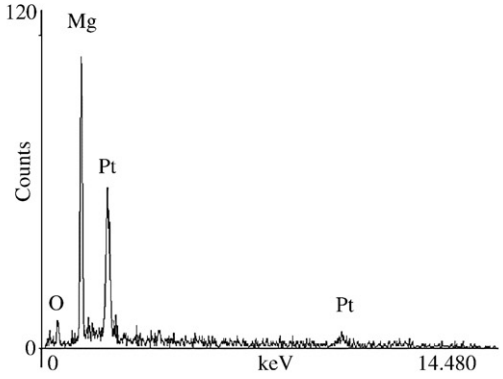

Fig. 9. SEM image of the fracture surface of MEA-46 hydrated in cement paste for 270 d cured in water at 40 °C.

(a) MEA-325 particle embedded in cement paste

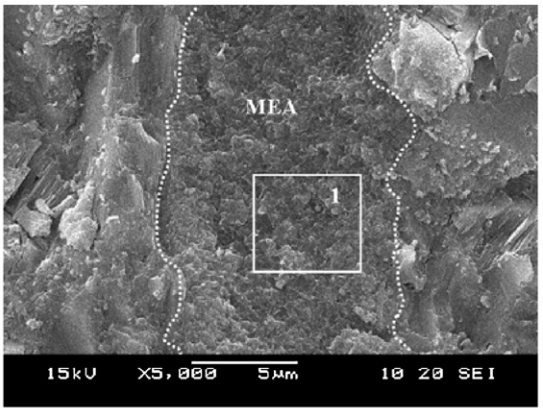

(b) Higher magnification image of zone 1

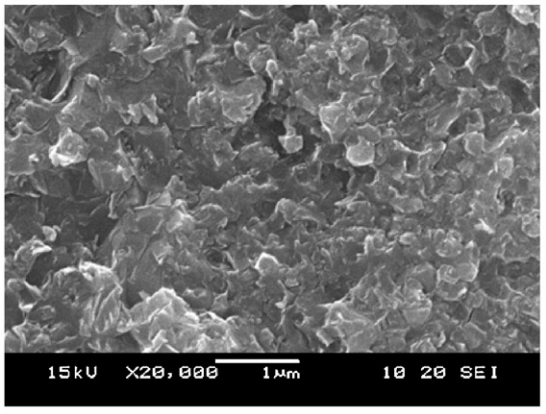

(c) EDS of zone 1

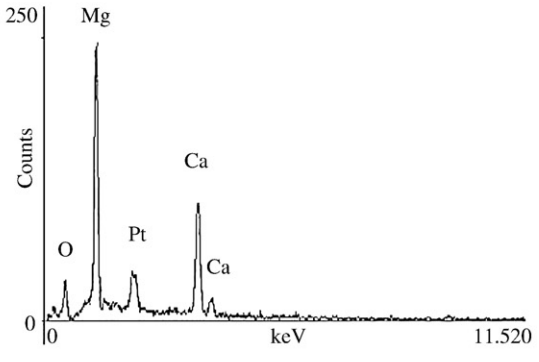

Fig. 10. SEM image of the fracture surface of MEA-325 hydrated in cement paste for 270 d cured in water at 40 °C.

hydration products, and there is obvious boundary between the MEA particle and cement matrix (Fig. 12(a)). At higher magnification, as seen in Fig. 12(b), it is obvious that, besides the hydration products $Mg(OH)_2$ formed on the surface of MEA particle, some hydration products were also formed around the sintered MgO grains in the interior portion of MEA particle and filled in the interior pores. What's more, some of the sintered MgO grains have been broken apart by the hydration products, which may be ascribed to the expansion caused by the hydration products formed at the boundary of MgO grains. The hydration products generated in or around the MEA particle will cause self-expansion of MAE particle, and the self-expansion of MEA particle is restrained by the surrounded cement matrix, thus inducing expansive stress and expanding the cement paste.

4. Discussion

According to the aforementioned results, the hydration characteristics of MEA in cement paste could be summarized as follows: (1) hydration occurs at the surface of MEA particle, interior pore surface, and the grain boundary of MgO. (2) $Mg(OH)_2$ is formed locally at or in a confined region near the site of MgO. (3) some of the hydration products are filled in the interior pores of MEA. According to these characteristics and taking into account of the interior pore structures of MEA, new hydration and expansion models could be proposed. As seen in Fig. 13, highly reactive MEA has porous structures and many interior pores exist in MEA particle (Fig. 13(a)). Due to the diffusion of pore solution into the interior pores, the hydration takes

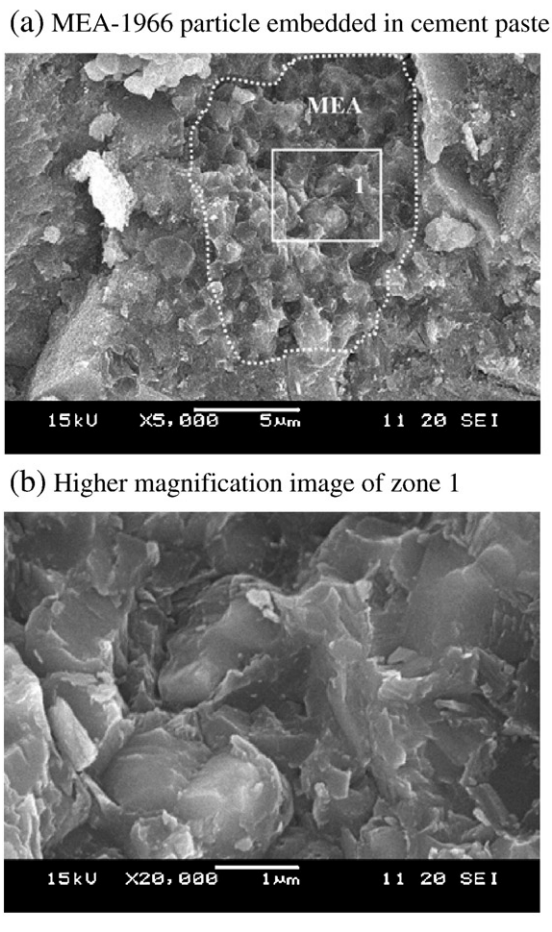

Fig. 11. SEM image of the fracture surface of MEA-1966 hydrated in cement paste for 270 d cured in water at 40 °C.

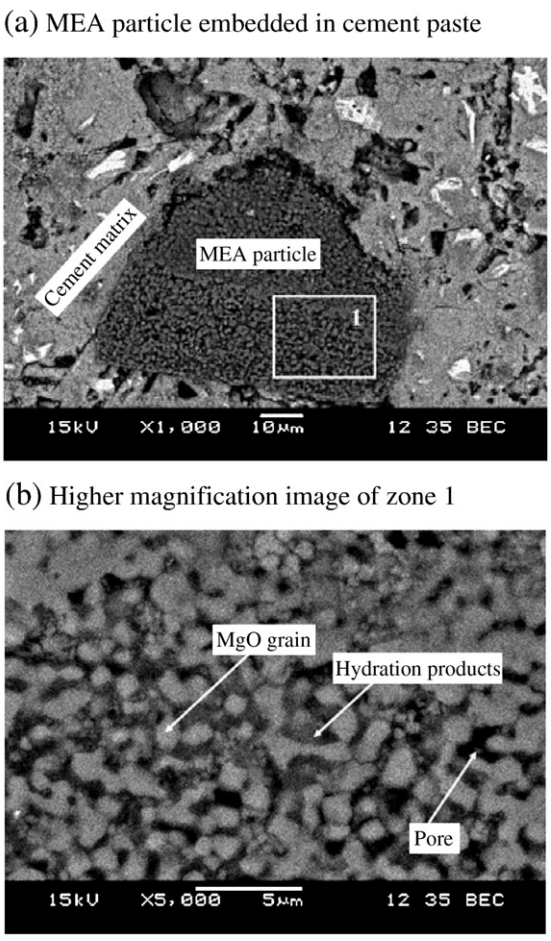

Fig. 12. Backscatter SEM image of MEA-1966 particle embedded in cement paste cured in 40 °C at the age of 270 d.

place both at the surface of MEA particle and the interior pore surface in MEA (Fig. 13(b)). With the reaction proceeds, hydration is continued towards the center of the MgO grain and simultaneously towards the boundary of MgO grain due to its relative high free energy [21,22]. At the presence of OH^-, supersaturated solution of Mg^{2+} and OH^- is formed in a confined region at the reaction site, and thus the $Mg(OH)_2$ is localized at or around the reaction site. The interior pores of MEA provide some room for the accommodation of $Mg(OH)_2$, and some of the hydration products are filled into the pores (Fig. 13(c)). Further formed products may cause the volume expansion of MEA particle (Fig. 13(c)). However, it is not a necessary condition for the pore to be filled completely by the hydration products to produce expansion. Some research indicated that crystallization in porous materials may also generate crystal growth pressure, resulting in expansion of the materials [23]. Hydration products formed at the grain boundary will cause larger expansion due to no or smaller room for the expansion accommodation at the boundary [21,22]. As the hydration proceeds, the sintered MgO grains in MEA particle are broken apart due to the expansion generated at the grain boundary, thus enlarging the total reaction surface area and accelerating the hydration and expansion (Fig. 13(d)).

For the MEA with low activity, as shown in Fig. 14, the interior pores and specific surface area are reduced (Fig. 14(a)). Thus the hydration at early age is slow, and the hydration at the grain boundary of MgO may play a more important role in the hydration and expansion of MEA (Fig. 14(b) and (c)). After a given period (generally called induction period), the hydration products formed at the MgO grain boundary induce enough expansive force to break apart the sintered MgO grains, enlarging the reaction surface area, thus accelerating the hydration and causing rapider expansion (Fig. 14(d)). This may be corresponding to the knee points that occur in the expansion curves of cement paste containing MEA-1266 and MEA-1966 (Fig. 8(b)). The lower the activity of MEA is, the longer time may be taken for the disaggregation of sintered MgO grains, and thus longer induction period is needed for the accelerated hydration and expansion. Compared to MEA with high activity, MEA with low activity has less interior pores and thus smaller room could be provided for the expansion accommodation. Consequently, more hydration products may be contributed to the self-expansion of MEA, inducing larger self-expansion of MEA and hence larger expansion of cement paste.

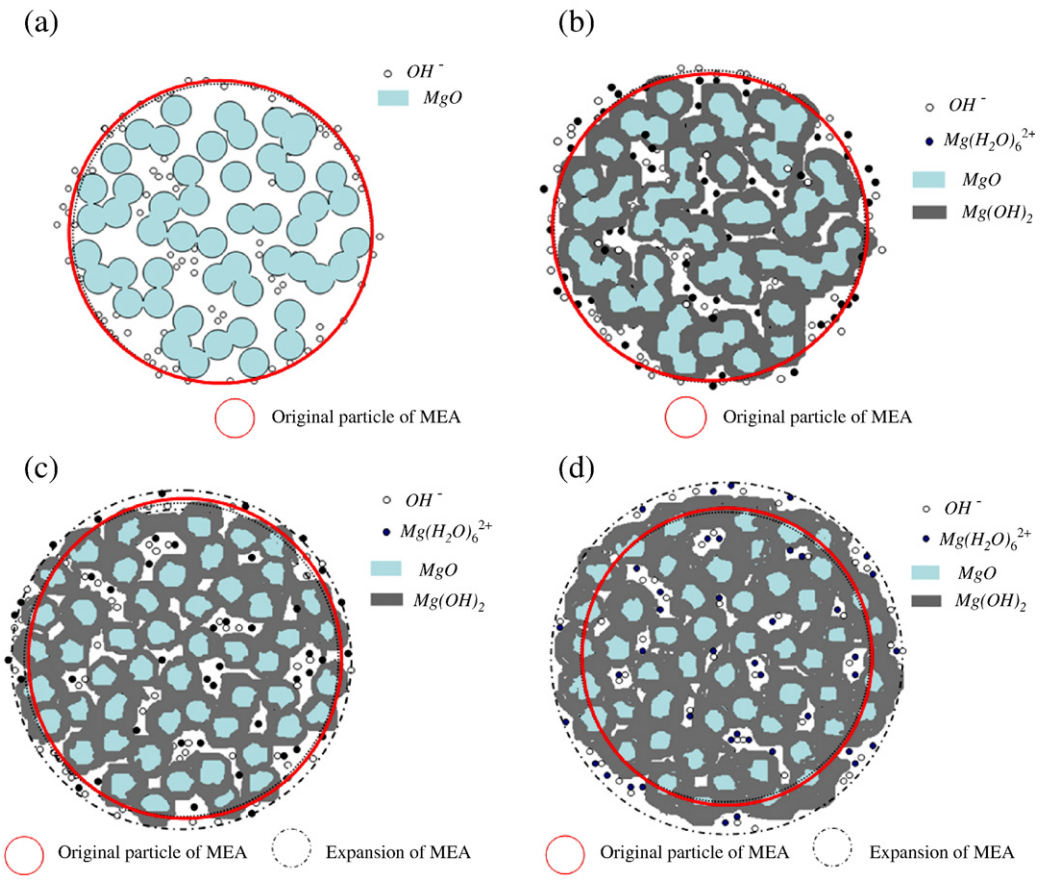

Fig. 13. Hydration and expansion model of the porous MEA with high activity in the cement paste.

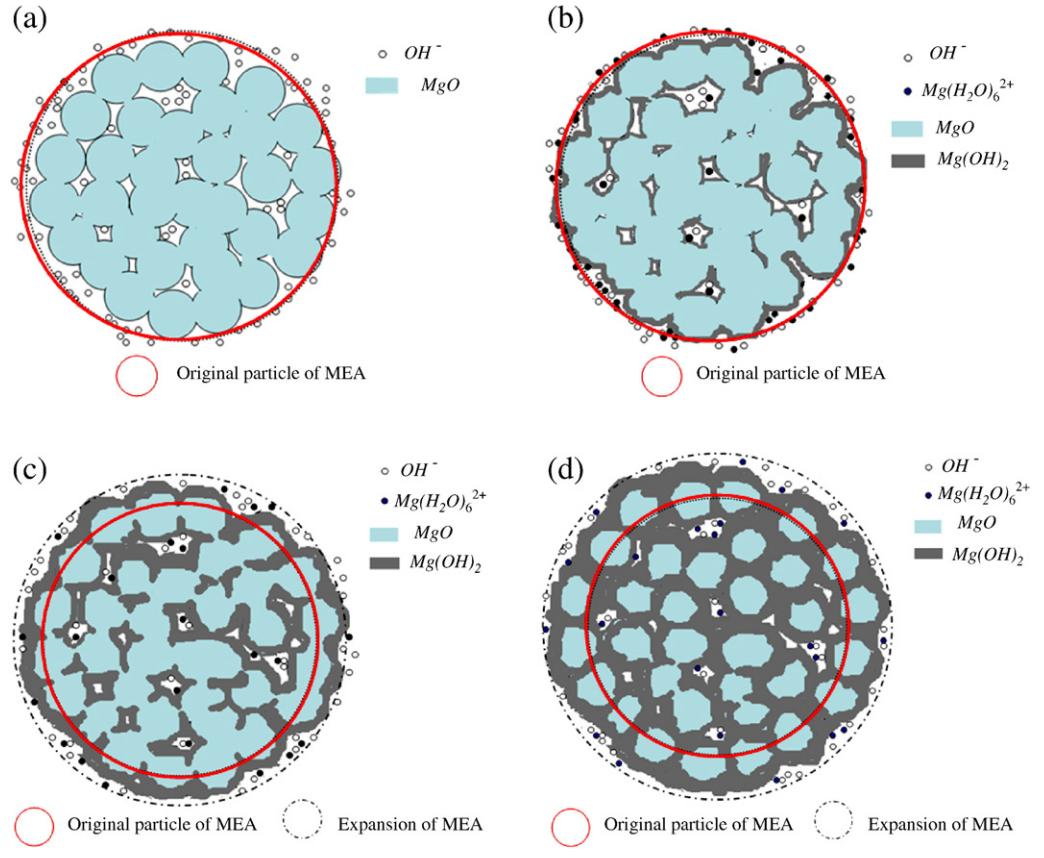

Fig. 14. Hydration and expansion model of the less porous MEA with low activity in the cement paste.

According to the model, the results that MEA prepared under different calcination conditions have different expansion properties could be explained. Two factors are thought to be responsible for the variation in the expansion properties of MEA. The first is the hydration activity. MEA with low activity hydrates more slowly at early age, and thus less MgO is hydrated and causes smaller expansion. Whereas at late age, more MgO is hydrated, thus causing larger expansion. For MEA with high activity, more MgO is hydrated at early age, thus causing rapider expansion. Less MgO is hydrated and hence less expansion is generated at the late age. Another important factor is the microstructure of MEA. As less interior pores are contained in the MEA with lower activity, hydration at grain boundary plays a more important role and smaller room could be provided for the expansion accommodation, hence larger expansion may be caused. It is also understandable from a macroscopical point of view that, for the same addition of MEA in cement paste (by mass of cement), as MEA with lower activity has larger density, less space originally occupied by the unhydrated MEA particle is provided for the accommodation of the hydration products, and therefore larger "ultimate" expansion may be caused.

5. Conclusions

Single MEA particle consists of many aggregated MgO grains, and these grains are sintered at the high temperature during calcining process. The intrinsic effect of calcination temperature and residence time on the expansion of MEA is attributed to its influence on the microstructures of MEA, such as the crystal grain size of MgO, pore structures, and specific surface area. Both of the specific surface area and the activity of MgO grain influence the hydration activity of MEA, and the latter may play a more important role. Higher calcination temperature and longer residence time will cause grain growth of MgO, thus decrease in inner pore volume and specific surface area, thus decreasing the hydration activity of MEA.

The self-expansion of MEA particle due to the hydration of MgO grains in MEA is the essential cause of the expansion of cement paste. The expansion property of MEA depends on its hydration activity and microstructure. MEA with high activity hydrates rapidly and thus produce fast expansion at early age, and short time is needed to reach the "ultimate" expansion. MEA with low activity will hydrate slowly and cause slow expansion at early age, but after an induction period, the sintered MgO grains are taken apart by the expansion at the grain boundary, increasing the reaction area and thus accelerating the hydration and the corresponding expansion. The lower the activity of MEA is, the longer induction period and larger "ultimate" expansion at late age will be produced.

According to the results obtained in this work, the expansion properties of MEA could be regulated by controlling its microstructures and hydration activity through changing the calcining temperature and residence time, which providing a principle for develop series kinds of MEA with various expansion properties.

Acknowledgement

This work is financially supported by the National Basic Research Program of China, namely the "973" Program (Grant No. 2009CB62310505). And the assistant work by Mr. X. Cui is gratefully appreciated.

References

[1] D.P. Bentz, O.M. Jensen, Mitigation strategies for autogenous shrinkage cracking, Cem. Concr. Compos. 26 (2004) 677–685.
[2] S. Nagataki, H. Gomi, Expansive admixtures, Cem. Concr. Compos. 21 (11) (1998) 163–170.
[3] R.K. Frederick, C.L. Bentley, W.W. Walker, J.A. Holland, Shrinkage-compensating concrete pavements perform well, Concr. Int. 1 (2006) 47–51.
[4] P. Yan, F. Zheng, et al., Relationship between delayed ettringite formation and delayed expansion in massive shrinkage-compensating concrete[J], Cem. Concr. Compos. 26 (2004) 687–693.
[5] P. Yan, X. Qin, The effect of expansive agent and possibility of delayed ettringite formation in shrinkage-compensating massive concrete[J], Cem. Concr. Res. 31 (2001) 335–337.
[6] P.K. Mehta, History and status of performance tests for evaluation of soundness of cements, Cement standards—Evolution and Trends, Am Soc Test Mater, vol. 663, ASTM STP, 1978.
[7] P.K. Mehta, D. Pirtz, Magnesium oxide additive for producing selfstress in mass concrete, 7th Int Congr Chem Cem. VO. III Paris, 1980, pp. v6–v9.
[8] Z. Cao, J. Xu, Dam construction technology using MgO concrete, China Electric Power Press, Beijing, 2003.
[9] X. Wang, Hydration and Expansion of MgO and the Preparation and Performance of the Novel MgO — type Expansive Agent, PhD thesis, Nanjing, 2002.
[10] L. Xu, M. Deng, Dolomite used as raw material to produce MgO-based expansive agent[J], Cem. Concr. Res. 35 (2005) 1480–1485.
[11] S. Chatterji, Mechanism of expansion of concrete due to the presence of dead-burnt CaO and MgO[J], Cem. Concr. Res. 25 (1) (1995) 51–56.
[12] Min Deng, Dongwen Hong, Xianghui Lan, Mingshu Tang, Mechanism of expansion in hardened cement pastes with dead-burnt free lime, Cem. Concr. Res. 25 (2) (1995) 440–448.
[13] Min Deng, Xuehua Cui, Yuanzhan Liu, Mingshu Tang, Expansive mechnismof magnesia as an additive of cement, J. Nanjing Inst. Chem. Technol. 12 (4) (1990) 1–11.
[14] C. Suryanarayana, M. Grant Norton, X-ray diffraction — a practical approach, Plenum Press, New York, 1998 212 pp.
[15] GB/T 208-94, Standard test method for cement density [S], 1994.
[16] K.O. Kjellsen, A. Monsφy, K. Isachsen, R.J. Detwiler, Preparation of flat-polished specimens for SEM-backscattered electron imaging and X-ray microanalysis — importance of epoxy impregnation, Cem. Concr. Res. 33 (4) (2003) 611–616.
[17] Sagvi Kleiman, Rachman Chaim, Thermal stability of MgO nanoparticles, Mater. Lett. 61 (2007) 4489–4491.
[18] W. Sun, C. Cui, H. Zhang, K. Cui, Relationship between crystalline size and lattice distortion of MgO and its activity, J. Wuhan Univ. Technol. 13 (4) (1991) 21–24.
[19] R.A. Wogelius, K. Refson, D.G. Fraser, G.W. Grime, J.P. Goff, Periclase surface hydroxylation during dissolution, Geochim. Cosmochim. Acta 59 (9) (1995) 1875–1881.
[20] J. Lv, L. Qiu, B. Qu, Controlled growth of three morphological structures of magnesium hydroxide nanoparticles by wet precipitation method[J], J. Cryst. Growth 267 (2004) 676–684.
[21] R. Salomão, L.R.M. Bittencourt, V.C. Pandolfelli, A novel approach for magnesia hydration assessment in fractory castables[J], Ceram. Int. 33 (2007) 803–810.
[22] A. Kitamura, K. Onizuka, K. Tanaka, Hydration characteristics of magnesia [J], Taikabutsu Overseas 16 (3) (1995) 3–11.
[23] S. Chatterji, Aspects of generation of destructive crystal growth pressure, J. Cryst. Growth 277 (2005) 566–577.